

Spatial Correlation Functions of one-dimensional Bose gases at Equilibrium

N.P. Proukakis

*School of Mathematics and Statistics, University of Newcastle,
Merz Court, Newcastle NE1 7RU, United Kingdom*

The dependence of the three lowest order spatial correlation functions of a harmonically confined Bose gas on temperature and interaction strength is presented at equilibrium. Our analysis is based on a stochastic Langevin equation for the order parameter of a weakly-interacting gas. Comparison of the predicted first order correlation functions to those of appropriate mean field theories demonstrates the potentially crucial role of density fluctuations on the equilibrium coherence length. Furthermore, the change in both coherence length and shape of the correlation function, from gaussian to exponential, with increasing temperature is quantified. Moreover, the presented results for higher order correlation functions are shown to be in agreement with existing predictions. Appropriate consideration of density-density correlations is shown to facilitate a precise determination of quasi-condensate density profiles, providing an alternative approach to the bimodal density fits typically used experimentally.

PACS numbers: 03.75.Hh, 05.30.Jp, 03.75.Nt

I. INTRODUCTION

The appearance of coherence in a system, which is central to our understanding of laser and matter wave physics, depends on the interplay between various parameters, such as temperature, interaction strength, confinement, and dimensionality. In particular, in the recently achieved confined weakly-interacting quasi-one-dimensional Bose gases in harmonic traps [1, 2, 3, 4, 5, 6], dipole traps [7, 8] and atom chips [9, 10, 11, 12, 13, 14, 15, 16, 17, 18, 19] coherence can only be maintained across the entire spatial extent of the system at a sufficiently low temperature, which is however much lower than the ‘critical temperature’ for the onset of quantum degeneracy. At intermediate temperatures, long wavelength fluctuations in the phase, restrict the coherence to smaller regions [20, 21, 22, 23, 24, 25, 26, 27, 28, 29, 30, 31, 32]. This effect has already been observed experimentally in very elongated three-dimensional Bose-Einstein Condensates [3, 4, 5, 6, 33, 34, 35].

In his seminal work [36], Glauber characterised the coherence of a system by means of a set of normalised correlation functions. Typically, the few ‘lowest order’ correlation functions are enough to characterise the coherence of a system [37, 38]. Perhaps the most important correlation function is the first order correlation function, referred to in condensed matter literature as the off-diagonal one-body density matrix. In an atomic gas above the degeneracy temperature, this quantity decays rapidly to zero, on a scale comparable to the atomic de Broglie wavelength (see, e.g., [39]). In the opposite extreme, when this quantity tends to a nonzero plateau, the system becomes coherent and is said to contain a Bose-Einstein Condensate (BEC). In degenerate one-dimensional (1D) gases, however, an intermediate state exists, in which the off-diagonal one-body density matrix does decay to zero within the system size, but at a much slower rate. In this regime, the system is said to contain a quasi-condensate [20].

The phase coherence properties of such trapped quasi-condensates were first investigated by Petrov et al. [21] in the low temperature limit, where quasi-condensate depletion can be treated as negligible. A number of alternative mean field approaches have appeared in the literature since [22, 23, 24, 25, 26, 27, 28, 29, 30, 31, 32, 40, 41]. In particular, the theory of Andersen et al. [22] treats both phase and density fluctuations in a self-consistent manner, thus providing the natural extension of the theory of Petrov et al. [21] to finite temperatures. Using this theory, we constructed the universal one-dimensional (1D) phase diagram in the weakly-interacting regime [24]. We also showed that inclusion of density fluctuations can potentially lead to a significant decrease in the equilibrium coherence length of a trapped quasi-condensate [25]. Although initial experiments performed to address this question found no such effect within their experimental resolution [4, 5, 6, 42], we argued that the apparent insensitivity of the (suitably scaled) coherence length on density fluctuations only arises in the regime $T_\phi \ll T_c$, in which all experiments to date have been performed, where T_ϕ is the characteristic temperature for phase fluctuations, and T_c is the ‘critical temperature’ for the onset of (quasi)condensation. In fact, despite a relatively weak coupling between density and phase fluctuations in most experiments, the first evidence of such coupling may have actually been recently observed [34]. The optimum conditions for the unequivocal experimental demonstration of such coupling between density and phase fluctuations was laid out in [25].

In this paper, we present results for the three lowest order spatial correlation functions at equilibrium, based on the stochastic Langevin treatment of Stoof [43, 44]. Where appropriate, these results are compared and contrasted to predictions of various mean field theories [21, 22, 26, 45, 46]. Firstly, we discuss the dependence of a suitably-defined equilibrium coherence length on temperature. Predictions of the present treatment are shown to be in full agreement with the mean field

theory of Andersen et al. [22], which includes density fluctuations in an *ab initio* manner, thus complementing and extending earlier related work [23]. Furthermore, the present work provides additional evidence to support our earlier claim [25] (based on mean field theory) that the coherence length is indeed sensitive to density fluctuations and quasi-condensate depletion in realistic parameter regimes. The spatial variation of the off-diagonal first order correlation function with distance z from the trap centre ($z = 0$) is evaluated in two different ways, corresponding experimentally to the particular atomic interference experiment that could be performed: In the first approach, atoms at the centre are numerically ‘interfered’ with atoms at a distance z from the trap centre, whereas the other approach ‘interferes’ atoms located symmetrically about the trap centre, i.e., at points $\pm z/2$. Good agreement is found between these two approaches within the quasi-condensate region. The interplay between quasi-condensation and ‘true’ condensation is known to be manifested, not only in the change of the scaled coherence length, but also in the shape of the first order correlation function, which changes smoothly from exponential to gaussian [29]. Analysing the correlation functions obtained by the stochastic approach at different temperatures, we model the interplay between such behaviour by two parameters, the first one controlling the shape of the function, and the second representing an appropriately-defined coherence length, which decreases uniformly with increasing temperature.

Higher order density-density correlation functions contain crucial information regarding the system’s coherence, and determination of such correlations (indirectly via measurement of the collisional interaction energy [47, 48, 49], or the three-body inelastic loss rate [50, 51]) has played a key role in unequivocally demonstrating the experimental observation of BEC in ultracold 3D bosonic atomic gases. Moreover, second order correlation functions have been well-studied in the context of photon statistics in the Hanbury-Brown-Twiss experiment [52], to discriminate between thermal and coherent light fields [37, 38], and a similar technique was recently used to experimentally determine the phase coherence length of a trapped elongated quasi-condensate [5, 33]. Furthermore, spatial two-body correlations have been observed in expanding atom clouds [53, 54] and atoms produced from molecular breakup [55], whereas temporal correlations were measured in continuously outcoupled atom lasers [56]. This paper additionally investigates in detail the dependence of the second and third order spatial correlation functions in confined weakly-interacting 1D Bose gases on temperature and interaction strength. The second order correlation function has already been discussed in the weakly-interacting regime in [45], with the crossover to the strongly-interacting regime presented in [46, 57], and our results reveal good agreement with such treatments in the appropriate regimes.

Density-density correlations are also used to directly determine the amount of quasi-condensation present in

a system at any given instant. Although already applied to study quasi-condensate growth on an atom chip [58], the details of this technique were not explicitly presented in our earlier work. In our opinion, this approach provides the most direct method that can be experimentally applied to obtain an unequivocal determination of quasi-condensate density profiles. In addition to providing an alternative to the conventional bimodal density fits, the advantage of experimentally obtaining the quasi-condensate density by the proposed method is that it is not subject to any potential limitations of the particular theory used to analyze the experimental data. This technique can be readily applied to existing experiments which performed *in situ* measurements of density fluctuations of quasi-1D Bose gases at equilibrium [35].

This paper is structured as follows: Sec. II briefly outlines the stochastic approach and other mean field theories to which the results are compared (see also Appendix A). Sec. III discusses the first order correlation function, focusing on the dependence of an appropriately defined coherence length on temperature (Sec. III A), and on method of evaluation (Sec. III B); moreover, Sec. III C analyses the crossover in the shape of the first order correlation function with decreasing temperature. Sec. IV discusses the dependence of higher-order density-density correlation functions on position and temperature (Sec. IV A) and effective interaction strength (Sec. IV B). Sec. V expounds how measurement of density-density correlations can provide an unequivocal determination of quasi-condensate density, which is demonstrated by means of suitable examples. Finally, Sec. VI summarises the main results of this paper.

II. LOW-DIMENSIONAL THEORIES

We start by reviewing the stochastic approach which will be used to evaluate all correlation functions presented in this work, and also briefly outlining the particular mean field theories against which our results will be tested.

A. Stochastic Langevin Approach

The stochastic Langevin theory of Stoof [43, 44] is a non-equilibrium approach, in which the system dynamics is obtained via a Langevin equation governing the evolution of the quasi-condensate order parameter $\Phi(z, t)$, given by [44]

$$i\hbar \frac{\partial \Phi(z, t)}{\partial t} = \left[-\frac{\hbar^2 \nabla^2}{2m} + V^{\text{ext}}(z) - \mu - iR(z, t) + g|\Phi(z, t)|^2 \right] \Phi(z, t) + \eta(z, t). \quad (1)$$

In the present work, this equation is applied to study the growth of a 1D degenerate atomic gas in contact with

a thermal cloud which acts as its heat bath. The numerical implementation of this scheme, along with further details, are discussed in Refs. [44, 59], while alternative but related approaches can be found in Refs. [45, 60, 61, 62, 63].

In addition to the usual kinetic, potential and interaction terms appearing within the square brackets of Eq. (1), Stoof's Langevin equation contains the contribution $iR(z, t)$, which describes pumping of the one-dimensional gas from the surrounding thermal reservoir. In the classical approximation imposed here for numerical simplicity, whereby the non-condensed 1D atomic cloud relaxes to the 'classical' value $N(\varepsilon) = [\beta(\varepsilon - \mu)]^{-1}$, the above pumping term obeys

$$iR(z, t) = -\frac{\beta}{4}\hbar\Sigma^K(z) \times \left(-\frac{\hbar^2\nabla^2}{2m} + V^{\text{ext}}(z) - \mu + g|\Phi(z, t)|^2 \right). \quad (2)$$

The term $\eta(z, t)$ corresponds to associated noise arising from the random nature of collisions occurring in the system. This noise term has Gaussian correlations of the form

$$\langle \eta^*(z, t)\eta(z', t') \rangle = \frac{i\hbar^2}{2}\Sigma^K(z)\delta(z - z')\delta(t - t'), \quad (3)$$

where $\langle \dots \rangle$ denotes averaging over the realizations of the noise. The quantities of Eqs. (2) and (3) depend on the one-dimensional Keldysh self-energy, $\hbar\Sigma^K(z)$, which accounts both for collisions that send a thermal atom into the quasi-condensate, and those which promote a quasi-condensate atom into the thermal cloud. The formulation of this theory ensures that the trapped gas relaxes to the correct equilibrium, in accordance with the fluctuation-dissipation theorem. The quantity μ appearing in Eqs. (1)-(2) describes the chemical potential of the system, whereas the external potential $V^{\text{ext}}(z)$ is treated as harmonic throughout this work, i.e. $V^{\text{ext}}(z) = m\omega_z^2 z^2/2$, where ω_z the corresponding confining frequency.

The quantity $\Phi(z, t)$ contains information about both mean field and fluctuations around it. It therefore implicitly includes both density and phase fluctuations, and acts as an approximation to the Bose field operator $\hat{\Psi}(z, t)$. Predictions of this theory are based upon averaging the Langevin field $\Phi(z, t)$ over different noise realizations. In particular, this theory enables an accurate determination of both diagonal and off-diagonal, spatial and temporal correlation functions of any order at any spatial and temporal coordinate. This is achieved by suitable numerical autocorrelation measurements of the 'order parameter' $\Phi(z, t)$, upon making the following identification

$$\langle \hat{\Psi}^\dagger(z, t)\hat{\Psi}(z', t') \rangle \rightarrow \langle \Phi^*(z, t)\Phi(z', t') \rangle. \quad (4)$$

In this paper we restrict our analysis to spatial correlations at equilibrium. To study these, we first evolve the

system for a sufficiently long time, t_{eq} , such that it relaxes to the correct equilibrium, before performing the desired same-time autocorrelation measurements. The first order normalised off-diagonal correlation function $g^{(1)}(0, z)$ associated with fluctuations in the quasi-condensate phase is thus calculated with respect to the centre of the trap via

$$g^{(1)}(0, z; t_{eq}) = \frac{\langle \Phi^*(0, t_{eq})\Phi(z, t_{eq}) \rangle}{\sqrt{\langle |\Phi(0, t_{eq})|^2 \rangle \langle |\Phi(z, t_{eq})|^2 \rangle}}. \quad (5)$$

Higher order correlation functions are also routinely obtained by a simple generalisation of the above formula. In particular, the second and third order correlation functions evaluated at the same spatial coordinate at equilibrium are numerically obtained via

$$g^{(2)}(z) = g^{(2)}(z, z, z, z; t_{eq}) = \frac{\langle |\Phi(z, t_{eq})|^4 \rangle}{\langle |\Phi(z, t_{eq})|^2 \rangle^2}, \quad (6)$$

and

$$g^{(3)}(z) = g^{(3)}(z, z, z, z, z, z; t_{eq}) = \frac{\langle |\Phi(z, t_{eq})|^6 \rangle}{\langle |\Phi(z, t_{eq})|^2 \rangle^3}, \quad (7)$$

respectively.

The above technique is very powerful, as it additionally enables a full non-equilibrium determination of coherence properties of the system, as demonstrated in [59]. This is of direct relevance to recent growth experiments [64] which will be investigated in future work.

B. Mean Field Theories

In our initial analysis, results of the first order correlation function, evaluated from Eq. (5), will be compared against corresponding results of a modified finite temperature mean field theory valid in low dimensions [22]. Although good agreement between these two theories has already been demonstrated [23], our aim here is to show that the agreement is *sufficiently sensitive* to *quantitatively* assess the role of density fluctuations on equilibrium coherence properties. In particular, under suitable realistic conditions, predictions of the stochastic approach are found to be in full agreement with the mean field theory which includes density fluctuations [22]. Importantly, however, the same stochastic predictions are shown to differ substantially from the limiting case of that mean field theory, in which density fluctuations are ignored [21]. This is an important remark, given that all coherence experiments (except [64]) have so far been analyzed in terms of theories which ignore density fluctuations.

Both mean field theories mentioned above are summarised in Appendix A. For our present purposes, it is sufficient to quote here the final expression for the first-order normalized correlation function $g^{(1)}(0, z)$, which is

given in terms of correlations of the phase operator, $\hat{\chi}(z)$ by

$$g^{(1)}(0, z) = e^{-\frac{1}{2}\langle[\hat{\chi}(z) - \hat{\chi}(0)]^2\rangle}. \quad (8)$$

The exponent of the above expression can be written in 1D as an appropriate sum over Legendre polynomials, with an additional prefactor which explicitly depends on the spatial extent of the quasi-condensate (see Eq. (A1)). The latter parameter is appropriately defined by a ‘temperature-dependent Thomas-Fermi radius’, $R_{\text{TF}}(T)$, whose size decreases with increasing temperature.

The low temperature theory of Petrov et al. [21] is obtained as a limiting case of this theory upon setting the quasicondensate depletion to zero, as demonstrated in [25]. To perform a calculation which is consistent with the ‘classical’ Langevin theory employed here, we again allow numerically the thermal part to relax to the classical value $N(\varepsilon) = [\beta(\varepsilon - \mu)]^{-1}$.

Let us now discuss the results of the theories presented above.

III. FIRST ORDER CORRELATION FUNCTION AT TRAP CENTRE

A. Temperature Dependence of $g^{(1)}(0, z)$

The spatial correlation function $g^{(1)}(0, z)$ evaluated at the trap centre at equilibrium by the stochastic approach is shown for two different temperatures by the brown (grey) lines in Fig. 1(a)-(b). Corresponding predictions based on the theory of Andersen et al. [22], i.e. including density fluctuations, and the theory of Petrov et al. [21], i.e. excluding density fluctuations, are shown respectively by the dashed and solid black lines. The spatial extent of all plotted curves is restricted to points within the temperature-dependent Thomas-Fermi (TF) radius $R_{\text{TF}}(T)$, which characterises the system size at each temperature (see also [23, 24]). As expected, the correlation function in the absence of density fluctuations is consistently higher than both other predictions (stochastic theory and mean field theory with density fluctuations), with this discrepancy becoming significant at higher temperatures. Importantly, these latter two theories show consistent behaviour over the entire temperature range, with only slight differences in the shapes of their predicted correlation functions at intermediate temperatures, presumably arising because the stochastic treatment does not predict gaussian behaviour close to the origin.

The good agreement between the stochastic approach and the mean field theory with density fluctuations becomes more evident in Figs. 1(c)-(d), which depict the temperature dependence of the correlation function suitably characterised by means of two independent determinations. Throughout this work, temperature is scaled to the ‘phase coherence’ temperature, $T_\phi = N(\hbar\omega_z)^2/\mu$ [21],

which marks the onset of phase fluctuations and roughly separates the regions of quasi-condensation and ‘true’ condensation. Here N denotes the quasi-condensate atom number, ω_z the confining frequency, and μ the 1D chemical potential.

The first approach we use here to compare the predictions for this correlation function over the entire temperature range, based on these three theories, is to investigate how the value of the correlation function halfway to the edge of the quasi-condensate, i.e. at $z = R_{\text{TF}}(T)/2$, varies as a function of temperature. This is shown in Fig. 1(c) against scaled temperature T/T_ϕ . In the quasi-condensate regime considered here, this quantity decreases smoothly to zero at a rate which depends critically on whether density fluctuations are included (circles, open squares), or not (filled squares), with both theories including density fluctuations showing very good agreement.

An alternative method for characterizing the temperature dependence of the correlation function is to appropriately extract a coherence length from it, scale this to the system size, and study its variation as a function of scaled temperature T/T_ϕ . A graph of this form is often compiled by experimentalists [34]. Here we choose to define the coherence length, L_{coh} , as the value of z at which the correlation function decays to half its original value, i.e. $g^{(1)}(0, L_{\text{coh}}) = 0.5$. We shall deal with a more suitable definition of the coherence length which also accounts for the changing shape of the correlation function in Sec. III C. In our numerical results, L_{coh} is scaled to the zero-temperature system size $R_{\text{TF}}(0)$, and its dependence on scaled temperature T/T_ϕ is shown in Fig. 1(d). Importantly, we find that all curves which include density fluctuations lie on a universal curve $L_{\text{coh}}/R_{\text{TF}}(0) = \exp(-T/T_\phi)$, whereas curves without density fluctuations (filled squares) lie considerably higher, indicating an overestimate of the actual equilibrium coherence length. As argued elsewhere [25], the shift between curves which include the coupling of phase and density fluctuations to those that do not, depends critically on the ratio of the phase coherence temperature T_ϕ , to the 1D ‘transition temperature’ T_c . Importantly, however, we note that the trend of the observed decrease of the coherence length due to density fluctuations is consistent with recent experimental findings [34].

All results presented in this paper are plotted in terms of suitably scaled parameters (lengths, temperatures), such that any dependence on the particular system details is removed. The underlying simulations were performed at constant chemical potential $\mu = 30\hbar\omega_z$ for a 1D gas of ^{23}Na atoms, of scattering length $a_{3\text{D}} = 2.75\text{nm}$, under longitudinal confinement of frequency $\omega_z = 2\pi \times 3.5\text{ Hz}$. The 1D interaction strength, denoted by g in Eq. (1), is given by $g = 4\pi\hbar^2\kappa/m$, where $\kappa = (m/2\pi\hbar)\omega_\perp a_{3\text{D}}$ is the 1D ‘coupling constant’ (or ‘inverse scattering length’) [65]. In our 1D simulations the value of κ is fixed by our choice of transverse confinement, taken here to be harmonic with frequency

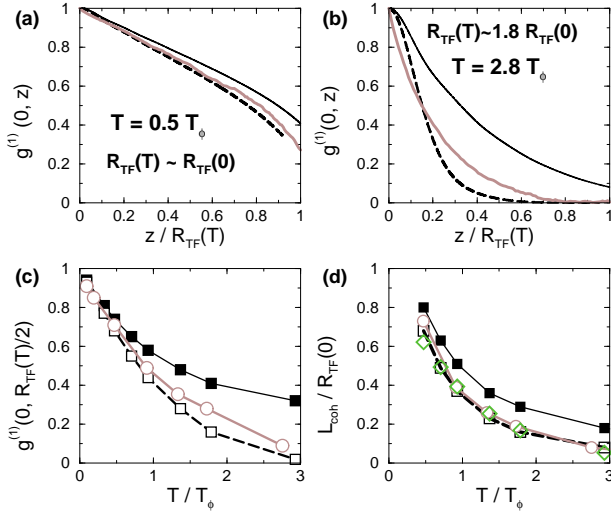


FIG. 1: (color online) (a)-(b) Normalized first order spatial correlation function $g^{(1)}(0, z)$ at equilibrium, obtained from the stochastic approach (solid brown/grey lines), and from mean-field theory with (dashed black) and without (solid black) inclusion of density fluctuations. Plotted temperatures correspond to $T/T_\phi \approx$ (a) 0.5, and (b) 2.8, with position z scaled to the effective temperature-dependent Thomas-Fermi radius $R_{TF}(T)$, the value of which decreases from (a) to (b). (The corresponding density profiles are shown in Fig. 6(a)-(b).) (c) Dependence of $g^{(1)}(0, z = R_{TF}(T)/2)$ on scaled temperature T/T_ϕ based on the stochastic approach (open circles) and modified mean field theory with (open squares) and without (filled squares) density fluctuations. (d) Dependence of the scaled coherence length $L_{coh}/R_{TF}(0)$ on scaled temperature T/T_ϕ for the 3 theories shown in (c). Here L_{coh} is defined by $g^{(1)}(0, L_{coh}/R_{TF}(0)) = 0.5$, where $R_{TF}(0)$ is the spatial extent of the condensate at $T = 0$. Only points corresponding to temperatures $T > T_\phi/2$ are plotted, since at lower temperatures the correlation function remains consistently above the value of 0.5, indicating full coherence. Green (grey) diamonds correspond to the curve $L_{coh}/R_{TF}(0) = \exp(-T/T_\phi)$. Plotted lines in (c)-(d) connect data points as a guide to the eye.

$\omega_\perp = 2\pi \times 120\text{Hz}$. Performing the simulation at fixed chemical potential leads to a slight variation in the atom numbers in the trap, in the range 18,500 – 24,000, for the considered temperature range, $10\text{nK} < T < 400\text{nK}$. An analogous variation would also be expected in experimental realisations at different temperatures and approximately fixed atom numbers. Accordingly, in the considered temperature range, the phase coherence temperature T_ϕ increases approximately linearly with increasing atom number (or, equivalently here, temperature T), from its initial value $T_\phi \sim 100\text{nK}$ to approximately $T_\phi \sim 125\text{nK}$.

B. Symmetrically Evaluated Correlation Function $g^{(1)}(-z/2, z/2)$

A number of current experiments are better suited to determining the correlation function symmetrically about a point, as done in the Hannover [5, 33] and Orsay experiments [6]. Our next task is therefore to investigate the extent to which the predictions discussed above depend on the precise method by which the correlation function is obtained. We will do this by comparing corresponding predictions at the trap centre, based on the stochastic theory.

The ‘symmetric’ correlation function at the trap centre is thus obtained at equilibrium via the following numerical autocorrelation

$$g^{(1)}(-z/2, z/2; t_{eq}) = \frac{\langle \Phi^*(-z/2, t_{eq}) \Phi(z/2, t_{eq}) \rangle}{\sqrt{\langle |\Phi(-z/2, t_{eq})|^2 \rangle \langle |\Phi(z/2, t_{eq})|^2 \rangle}} \quad (9)$$

which should be compared and contrasted to Eq. (5).

Correlation functions computed symmetrically via Eq. (9) are shown by the brown (grey) lines in Fig. 2(a) for four different values of T/T_ϕ . These are compared to corresponding correlation functions $g^{(1)}(0, z)$ of Eq. (5) (black). We find that, for a given temperature which fixes the density profile, these two correlation functions are indistinguishable in a broad region close to the trap centre. Some differences do, however, arise towards the edge of the quasi-condensate, and beyond, for certain temperatures just below the phase coherence temperature T_ϕ . A slower decrease of the symmetrically computed correlation function $g^{(1)}(-z/2, z/2)$ is anticipated in this region, since the different methods of evaluation used imply that the considered correlation functions will decay to zero at different points, respectively at $z \approx R_{TF}(T)$ for $g^{(1)}(0, z)$ and $z \approx 2R_{TF}(T)$ for $g^{(1)}(-z/2, z/2)$.

For sufficiently low temperatures, as in Fig. 2(a)(i), the agreement between the two different determinations of the correlation function is accurate almost up to the edges of the quasi-condensate (i.e., $z = R_{TF}(T)$), and the same holds deeply in the quasi-condensate regime shown in Fig. 2(a)(iv), for which the two independently determined correlation functions are practically indistinguishable. In fact, this equivalence remains nearly perfect over the entire temperature range, for spatial coordinates $z \leq R_{TF}(T)/2$. This is evident in Fig. 2(b) which compares the temperature dependence of the value of the correlation function at $z = R_{TF}(T)/2$, based on the two different determinations mentioned above. The reader is reminded that a similar determination of the coherence length was used in Fig. 1(c) to demonstrate the importance of density fluctuations. For completeness, Fig. 2(c) plots the effective system size, $R_{TF}(T)$, versus scaled temperature T/T_ϕ , demonstrating an approximately linear decrease with increasing temperature.

One might also consider performing the alternative analysis of Fig. 1(d), whereby the coherence length is defined by the spatial coordinate z , at which the first order

correlation function $g^{(1)}$ decays to the value of 0.5, with this value scaled to $R_{\text{TF}}(0)$. In this case, at low temperatures $T \leq T_\phi$, the two correlation functions are sensitive to their precise evaluation method, and the agreement between them would not be as good.

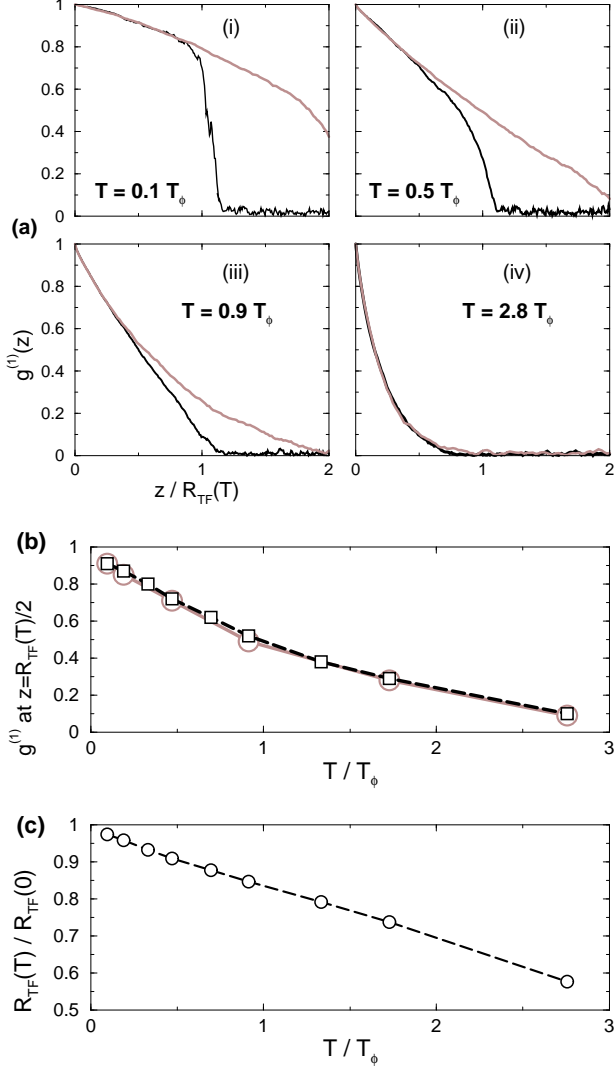


FIG. 2: (color online) (a) (i)-(iv) Spatial dependence of the normalised first order correlation function, calculated via the stochastic theory, under different autocorrelation measurements. Black lines denote the function $g^{(1)}(0, z)$ of Eq. (5), whereas brown (grey) lines show the symmetrically evaluated $g^{(1)}(-z/2, z/2)$ of Eq. (9). Plotted graphs correspond to temperatures $T/T_\phi \approx$ (i) 0.1, (ii) 0.5, (iii) 0.9, and (iv) 2.8, with z scaled throughout to the temperature-dependent system size $R_{\text{TF}}(T)$. (b) Value of the normalised first-order correlation function evaluated at $z = R_{\text{TF}}(T)/2$ from the trap centre, as a function of scaled temperature T/T_ϕ , obtained from $g^{(1)}(0, z)$ (brown/grey circles), and $g^{(1)}(-z/2, z/2)$ (black squares). (c) Dependence of $R_{\text{TF}}(T)$ on scaled temperature T/T_ϕ . Plotted lines in (b)-(c) are a guide to the eye.

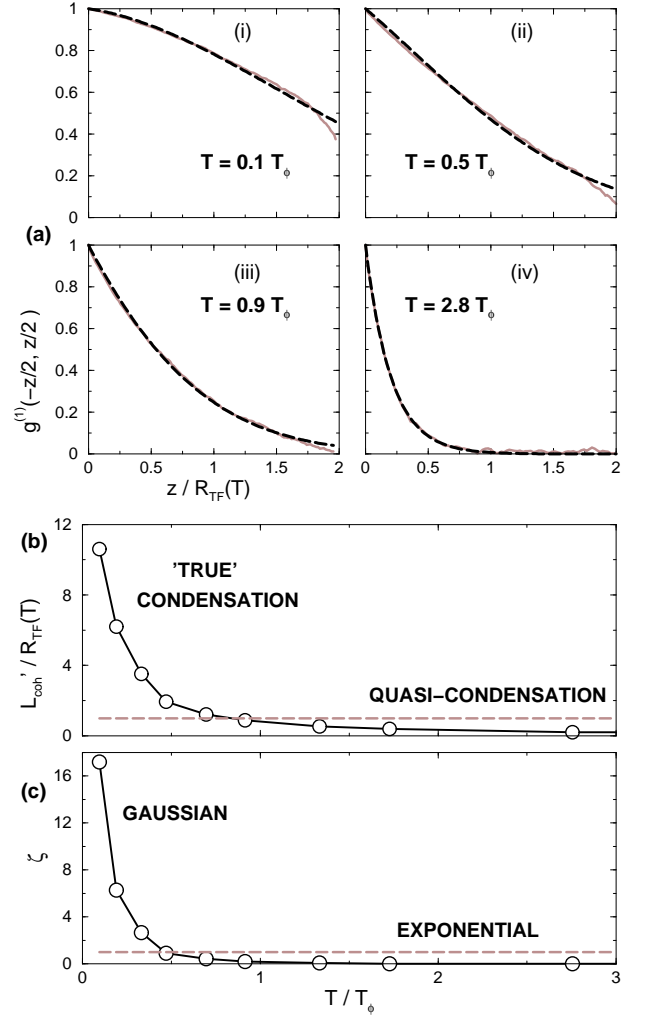


FIG. 3: (color online) (a) (i)-(iv) Symmetrically computed spatial correlation function $g^{(1)}(-z/2, z/2)$, where z is scaled to the temperature-dependent Thomas-Fermi radius $R_{\text{TF}}(T)$ (solid brown/grey), versus numerical fit by the function $f(z)$ of Eq. (10) (dashed black), for the graphs of Fig. 2(a). (b) Temperature dependence of the coherence length L'_{coh} (black circles) obtained by above fit, with L'_{coh} scaled to $R_{\text{TF}}(T)$, and temperature to T_ϕ . The dashed brown (grey) line highlights a coherence equal to the system size, i.e. $L'_{\text{coh}} = R_{\text{TF}}(T)$. (c) Corresponding dependence of the 'crossover' parameter ζ (black circles) determining the relative importance of exponential and gaussian contributions to the spatial correlation. The dashed brown (grey) line separates regions of predominantly gaussian behaviour ($\zeta \gg 1$), to those of exponential behaviour. Plotted solid lines in (b)-(c) are a guide to the eye.

C. Exponential vs. Gaussian Profiles

The presented analysis thus far has focused only on the 'global' loss of coherence with increasing temperature, without paying attention to the precise shape of the correlation function. The latter is known to vary from exponential to gaussian with decreasing tempera-

ture, indicating the crossover from quasi-condensation to ‘true’ condensation [29]. In this section we study the temperature crossover in the shape of this function in more detail, by means of our previously computed symmetric correlation function $g^{(1)}(-z/2, z/2)$. Since $g^{(1)}$ is known to be gaussian at $T = 0$ and exponential at temperatures $T > T_\phi$, we fit it, in the relevant region $z \leq 2R_{\text{TF}}(T)$, by a function $f(z)$ which provides a smooth crossover between the two shapes, of the form

$$f(z) = e^{-[(z/L'_{\text{coh}}) + \zeta(z/L'_{\text{coh}})^2]}. \quad (10)$$

The parameter ζ appearing above is a measure of how ‘gaussian’ or ‘exponential’ a particular profile is, while the chosen fit provides a unique definition of the coherence length, L'_{coh} , which decreases monotonically with increasing temperature, irrespective of the change in the profile’s shape.

The correlation functions $g^{(1)}(-z/2, z/2)$ for the four different temperatures discussed earlier are shown by the brown (grey) lines in Fig. 3(a); the corresponding fits based on Eq. (10) are plotted on the same figure by dashed black lines. Such fits enable us to study the dependence of the ‘crossover parameter’, ζ , and the coherence length, L'_{coh} , on temperature. In particular, the scaled coherence length $L'_{\text{coh}}/R_{\text{TF}}(T)$ and the ‘crossover’ parameter ζ are plotted against scaled temperature T/T_ϕ in Fig. 3(b)-(c). Note that a value of $\zeta = 0$ corresponds to a purely exponential correlation function, with the gaussian limit reached for $\zeta \gg 1$.

At low temperatures, $T < T_\phi$, we find that the coherence length L'_{coh} is comparable to, or larger than the quasi-condensate spatial extent, $R_{\text{TF}}(T)$, for that particular temperature, signalling the appearance of ‘true’ condensation. In this regime, the gaussian contribution has a larger weight, than the exponential term. Moreover, we find that the ratio in their relative contributions decreases with increasing temperature, with $\zeta \approx 1$ at the ‘crossover region’. Finally, as the temperature increases further, the system enters the quasi-condensate regime and the correlation function essentially acquires an exponential profile for temperatures $T > T_\phi$, consistent with experimental observations.

IV. HIGHER ORDER (DENSITY-DENSITY) CORRELATION FUNCTIONS

In this section we consider higher order correlation functions, which contain information about density-density correlations. These are considered at fixed points z and at equilibrium, with the subsequent analysis focusing on the correlation functions $g^{(2)}(z) = g^{(2)}(z, z, z, z; t_{\text{eq}})$, and $g^{(3)}(z) = g^{(3)}(z, z, z, z, z, z; t_{\text{eq}})$ of Eqs. (6)-(7) as a function of z for various temperatures.

A. Dependence on Temperature

The behaviour of $g^{(2)}(z)$ and $g^{(3)}(z)$ against z is shown for various temperatures in Figs. 4(a) and (b), with position scaled to the zero-temperature Thomas-Fermi radius, $R_{\text{TF}}(0)$. As expected, these functions have a lower bound of 1, occurring deep within the quasi-condensate region ($z \ll R_{\text{TF}}(0)$), and at sufficiently low temperatures, demonstrating full coherence. The corresponding upper bounds for these functions are $g^{(2)}(0) = 2! = 2$, and $g^{(3)}(0) = 3! = 6$, consistent with the observed values in 3D BECs [47, 48, 49, 50]. These values correspond to complete absence of coherence, and such incoherent thermal atoms are typically located outside the quasi-condensate region.

In particular, as $T \rightarrow 0$, both functions $g^{(2)}(z)$ and $g^{(3)}(z)$ tend towards step-like functions $g^{(n)}(z) = 1 + (n! - 1)\Theta(z)$ centered around $R_{\text{TF}}(0)$, with $\Theta(z) = 0$ for $z \leq R_{\text{TF}}(0)$ and 1 for $z > R_{\text{TF}}(0)$. As the temperature increases, we observe the following features, which are consistent with the results of [45]: Firstly, the central values $g^{(2)}(0)$ and $g^{(3)}(0)$ increase due to the increasing thermal component located at the trap centre; their dependence on temperature is shown in Fig. 4(c). Furthermore, the crossover between the quasi-condensate-dominated region $z < R_{\text{TF}}(T)$, and the purely thermal region $z > R_{\text{TF}}(T)$ becomes smoother, due to the increased presence of thermal atoms over the entire trap extent. Finally, the location of this crossover is shifted to smaller values of $z/R_{\text{TF}}(0)$, consistent with the decrease in the spatial extent $R_{\text{TF}}(T) < R_{\text{TF}}(0)$ of the quasi-condensate with increasing temperature.

Our findings for the temperature dependence of $g^{(2)}(0)$ in Fig. 4(c) are further compared to the analytical result of Kheruntsyan et al. [46, 57]. In their work, the interaction strength is parametrised in terms of the parameter $\gamma = mg/\hbar^2 n$, where m is the atomic mass, g the one-dimensional coupling constant, and n the density of the gas. In the regime $\gamma \ll 1$ considered here, they find the following temperature dependence (see Eq. (5.10) in Ref. [46])

$$g^{(2)}(0) = 1 + \frac{4\sqrt{2}}{3} \left(\frac{T}{T_d} \right) \quad (11)$$

where T_d is the degeneracy temperature, defined by $T_d = N\hbar\omega_z$, N is the number of quasi-condensate atoms and ω_z is the confining frequency. We apply this analytical formula to our numerical results by extracting the relevant parameter (T/T_d) from our stochastic simulations. The corresponding temperature dependence of $g^{(2)}(0)$ predicted by Eq. (11) is thus plotted by the brown (grey) triangles in Fig. 4(c). Thus there is good agreement between the stochastic and analytical theories in the temperature range considered here. However, the stochastic theory predicts an additional slight *reduction* in coherence, as manifested by the *higher* value of $g^{(2)}(0)$, with the extent of this reduction increasing with increasing temperature.

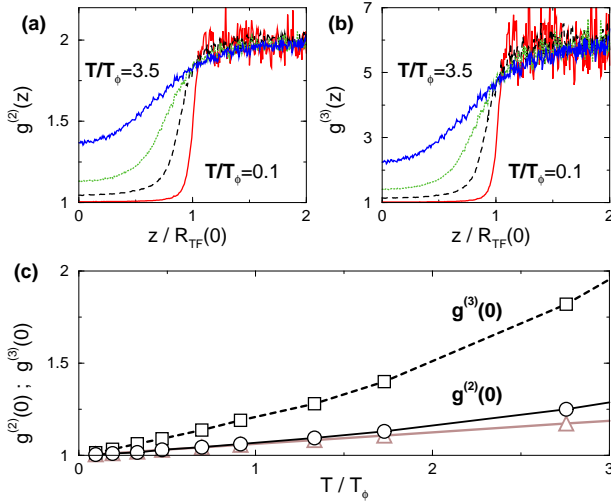


FIG. 4: (color online) (a)-(b) Spatial dependence of the (a) second, $g^{(2)}(z)$, and (b) third order, $g^{(3)}(z)$, equilibrium spatial correlation functions at the same point z , for various temperatures; from bottom to top $T/T_\phi \approx$: (i) 0.1, (ii) 0.7, (iii) 1.7, and (iv) 3.5. Distances are scaled to the zero temperature system size $R_{\text{TF}}(0)$. (c) Corresponding values of $g^{(2)}(0) = g^{(2)}(0, 0, 0, 0; t_{\text{eq}})$ (black circles) and $g^{(3)}(0) = g^{(3)}(0, 0, 0, 0, 0; t_{\text{eq}})$ (black squares) at trap centre as a function of temperature. Brown (grey) triangles indicate corresponding results for $g^{(2)}(0)$ based on Eq. (11). Plotted lines in (c) are a guide to the eye.

B. Dependence on Interaction Strength

Next, we investigate the dependence of the three-lowest order correlation functions on the effective 1D interaction strength at fixed temperature, with our analysis again restricted to the weakly-interacting regime $\gamma \ll 1$. As mentioned earlier, the 1D interaction strength can be parametrised in terms of the 1D coupling constant $\kappa = (m/2\pi\hbar)a_{3\text{D}}\omega_\perp$. This parameter can be changed either by tuning the 3D scattering length via Feshbach resonances [66, 67], or by modifying the transverse confinement, while keeping all other parameters fixed. Since an increase in the interaction strength causes a reduction of coherence, as demonstrated explicitly below, we have chosen to discuss here a rather low temperature example, with $T = 0.5T_\phi$, for which there is appreciable coherence in the system.

The dependence of the three lowest order correlation functions on coupling constant κ is shown in Fig. 5, with the coupling constant used thus far in our discussion, and in Figs. 1-4, henceforth denoted by κ_0 . Since temperature is kept fixed for all curves shown in this section, we have chosen here to scale distances to the quasi-condensate spatial extent at the given temperature $T = 0.5T_\phi$, based on the coupling constant κ_0 . For this particular coupling constant, the corresponding first order correlation functions were shown in Figs. 2(a)(ii) and 3(a)(ii) (note the different plot ranges), whereas higher

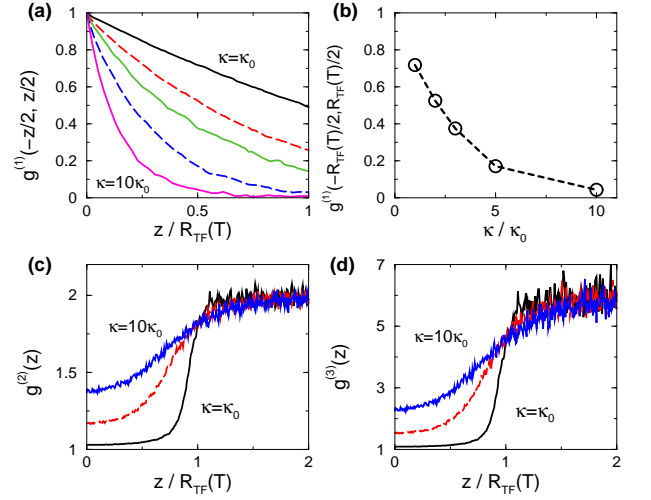


FIG. 5: (color online) Dependence of the three lowest order correlation functions on the effective 1D coupling constant κ at equilibrium for a fixed low temperature $T \approx 0.5T_\phi$: (a) Dependence of $g^{(1)}(-z/2, z/2)$ on κ as a function of position, for (from top to bottom) $\kappa/\kappa_0 = 1, 2, 3, 5$ and 10, where κ_0 is the value of the effective 1D coupling constant used in Figs. 1-4. (b) Dependence of $g^{(1)}(-z/2, z/2)$ at $z = R_{\text{TF}}(T)/2$ on κ/κ_0 , with the dashed line simply connecting the data points. (c)-(d) Second and third order spatial correlation functions at the same point and at equilibrium as a function of position, for an interaction strength (from bottom to top) $\kappa/\kappa_0 = 1, 5, 10$. Here, the value of the 1D coupling constant κ has been changed by modifying the transverse confinement from $\omega_\perp = 2\pi \times 120\text{Hz}$, to the values $\omega'_\perp/2\pi = 240, 360, 600$, and 1200 Hz. In this figure, all positions have been scaled to the spatial extent of the system at $T = 0.5T_\phi$ for a coupling constant $\kappa = \kappa_0$.

order correlation functions were plotted by the dashed black lines in Figs. 4(a)-(b).

The change in the correlation function $g^{(1)}(-z/2, z/2)$ as a function of position for different values of the 1D coupling constant is shown in Fig. 5(a). As evident, an increase in κ , from its previously considered value κ_0 , leads to a decrease in the coherence of the system. This is clearly portrayed in Fig. 5(b) showing the value of the correlation function at $z = R_{\text{TF}}(T)/2$ as a function of κ . This curve further demonstrates that full coherence is asymptotically approached in the limit of negligible interactions, i.e. as $\kappa \rightarrow 0$, as anticipated.

Figs. 5(c)-(d) show corresponding dependence of $g^{(2)}(z)$ and $g^{(3)}(z)$ on z for different interaction strengths, with top curves corresponding to a ten-fold increase in κ . Our analysis reveals that an increase of the interaction strength leads to an increase in the central values of the correlation function $g^{(2)}(0)$ and $g^{(3)}(0)$, and a more gradual crossover to incoherent behaviour outside the quasi-condensate region. Thus, qualitatively, an increase in the interaction strength produces the same effect on the system coherence as an increase in the temperature of the system.

V. DIRECT DETERMINATION OF QUASI-CONDENSATE PROFILES

The calculation of density-density correlations discussed previously enables the precise determination of the quasi-condensate density, to which we now turn our attention.

A. Methodology

To be able to identify the quasi-condensate part in our density profiles, we use the fact that the Langevin field $\Phi(z, t)$ essentially contains the physics of the Bose field operator $\hat{\Psi}(z, t)$. Such a correspondence has already been used in numerically evaluating the three lowest order correlation functions $g^{(1)}(\dots)$, $g^{(2)}(\dots)$, and $g^{(3)}(\dots)$ from Eqs. (5)-(7) in Secs. III and IV. At a given time, the total atomic density is obtained via

$$n(z) = \langle \hat{\Psi}^\dagger(z) \hat{\Psi}(z) \rangle \rightarrow \langle |\Phi(z)|^2 \rangle, \quad (12)$$

where the latter averaging is performed over different realizations of the noise.

In order to separate out quasi-condensate and thermal contributions, we impose the usual ‘decomposition’ of the Bose field operator into a ‘mean field part’ $\psi_0(z)$ and a ‘fluctuating part’ $\hat{\delta}(z)$, i.e.,

$$\hat{\Psi}(z) = \langle \hat{\Psi}(z) \rangle + \hat{\delta}(z) = \psi_0(z) + \hat{\delta}(z). \quad (13)$$

This directly enables us to split the atomic profile of Eq. (12) into a ‘quasi-condensate part’, $n_{\text{QC}}(z)$, and a ‘thermal part’, $n_{\text{T}}(z)$, via

$$n(z) = n_{\text{QC}}(z) + n_{\text{T}}(z) = |\psi_0(z)|^2 + \langle \hat{\delta}^\dagger(z) \hat{\delta}(z) \rangle. \quad (14)$$

We now seek to re-write these two components in terms of expressions involving same-time averages of multiple Bose field operators, since the latter quantities can be routinely evaluated within our numerical scheme. In particular, we note that the average over four Bose field operators at the same spatial coordinate (and same time) can be written as

$$\begin{aligned} \langle \hat{\Psi}^\dagger(z) \hat{\Psi}^\dagger(z) \hat{\Psi}(z) \hat{\Psi}(z) \rangle &= |\psi_0(z)|^4 \\ &+ 4 |\psi_0(z)|^2 \langle \hat{\delta}^\dagger(z) \hat{\delta}(z) \rangle + 2 \langle \hat{\delta}^\dagger(z) \hat{\delta}(z) \rangle^2 \end{aligned} \quad (15)$$

where we have used Wick’s theorem in the form

$$\langle \hat{\delta}^\dagger(z) \hat{\delta}^\dagger(z) \hat{\delta}(z) \hat{\delta}(z) \rangle = 2 \langle \hat{\delta}^\dagger(z) \hat{\delta}(z) \rangle^2. \quad (16)$$

At the same time, we make use of the following correspondence

$$\begin{aligned} \langle \hat{\Psi}^\dagger(z) \hat{\Psi}^\dagger(z) \hat{\Psi}(z) \hat{\Psi}(z) \rangle &\rightarrow \langle \Phi^*(z) \Phi^*(z) \Phi(z) \Phi(z) \rangle \\ &= \langle |\Phi(z)|^4 \rangle \end{aligned} \quad (17)$$

So, from Eqs. (12)-(17) it is easy to see that, in the region $z \leq R_{\text{TF}}(T)$ where a quasi-condensate exists, and therefore the above splitting into mean field and fluctuations is meaningful, the following relation holds

$$|\psi_0(z)|^4 = 2 \langle \hat{\Psi}^\dagger(z) \hat{\Psi}(z) \rangle^2 - \langle \hat{\Psi}^\dagger(z) \hat{\Psi}^\dagger(z) \hat{\Psi}(z) \hat{\Psi}(z) \rangle. \quad (18)$$

The quasi-condensate density $n_{\text{QC}}(z) = |\psi_0(z)|^2$ can hence be accurately determined in the range $z \leq R_{\text{TF}}(T)$ from our numerical scheme via

$$\begin{aligned} n_{\text{QC}}(z) &= \sqrt{2 \langle \hat{\Psi}^\dagger(z) \hat{\Psi}(z) \rangle^2 - \langle \hat{\Psi}^\dagger(z) \hat{\Psi}^\dagger(z) \hat{\Psi}(z) \hat{\Psi}(z) \rangle} \\ &\rightarrow \sqrt{2 \langle |\Phi(z)|^2 \rangle^2 - \langle |\Phi(z)|^4 \rangle}. \end{aligned} \quad (19)$$

Correspondingly, the profile of the thermal cloud, $n_{\text{T}}(z) = \langle \hat{\delta}^\dagger(z) \hat{\delta}(z) \rangle$ is directly obtained via

$$n_{\text{T}}(z) = \langle |\Phi(z)|^2 \rangle - n_{\text{QC}}(z). \quad (20)$$

This approach has already been used (but not commented upon) in parallel work discussing quasi-condensate growth on an atom chip [58].

Note that an alternative approach to determine quasi-condensate density profiles has been recently discussed in [45], based on the projected Gross-Pitaevskii scheme [62].

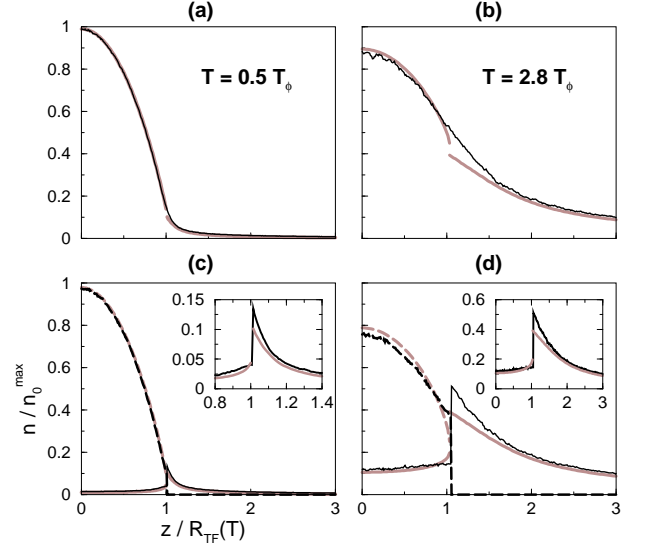


FIG. 6: (a)-(b) Total density profiles, scaled to the $T = 0$ peak central density, n_0^{max} , as obtained from the stochastic approach (black), and mean field theory with density fluctuations (brown/grey) corresponding to the correlation functions plotted Fig. 1(a)-(b). (c)-(d) Corresponding quasi-condensate (dashed) versus thermal cloud profiles (solid). Insets: Thermal cloud profiles around their maxima, $z = R_{\text{TF}}(T)$. All graphs are scaled to the temperature-dependent Thomas-Fermi radius $R_{\text{TF}}(T)$ for the particular temperature, and are based on the coupling constant κ_0 of Figs. 1-4.

B. Results

To apply the above method, we start by plotting the total density profiles at two different temperatures, above and below T_ϕ in Fig. 6(a)-(b). These figures depict the good agreement between the stochastic and mean field approaches commented upon in earlier work [23]. In this paper such an analogy is extended much further, by directly comparing quasi-condensate and thermal profiles predicted by these two theories, as shown in Fig. 6(c)-(d). The quasi-condensate density is evaluated in the stochastic theory by Eq. (19) within the range $0 \leq z \leq R_{\text{TF}}(T)$, and is zero elsewhere.

In order to make a meaningful comparison between these distinct approaches, at any given temperature, the same temperature-dependent Thomas-Fermi radius is used for both theories, with $R_{\text{TF}}(T)$ evaluated from the mean field theory. Dashed lines in Figs. 6(c)-(d) depict the quasi-condensate, as evaluated from the stochastic (black) and the mean field theory (brown/grey), whereas solid lines show corresponding thermal cloud distributions. The latter are highlighted in the insets around their respective maxima, located at the quasi-condensate edges $z = R_{\text{TF}}(T)$. The agreement between the predicted profiles is excellent, and remains so over the entire temperature range considered.

The approach presented here further enables the direct determination of the equilibrium quasi-condensate fraction at any temperature. In particular, we note that the quasi-condensate fraction is found to decrease approximately linearly with increasing temperature.

C. Application to Experiments

Experiments with quasi-condensates typically rely on bimodal density fits to determine important parameters such as the quasi-condensate spatial extent and quasi-condensate fraction at a given temperature. The procedure described above provides a direct alternative way of obtaining an unequivocal, theory-independent determination of quasi-condensate and thermal density profiles in quasi-1D experiments.

In order to perform such an analysis experimentally, one must simultaneously obtain both the total atomic density profiles $n(z) = \langle |\Phi(z)|^2 \rangle$, as done routinely, as well as the density-density correlations $\langle n^2(z) \rangle = \langle |\Phi(z)|^4 \rangle$ at various points across the entire trap. This experiment should ideally be performed in situ, which is within current experimental reach [35], in order to avoid the coupling of density and phase fluctuations occurring in the usual time-of-flight expansion stage [3, 6].

VI. CONCLUSIONS

In conclusion, we carried out a systematic analysis of the dependence of the three lowest order correlation

functions of a one-dimensional ultracold atomic gas on temperature and effective interaction strength, by means of a stochastic Langevin approach in the ‘classical’ approximation. Our discussion was limited to the weakly-interacting regime ($\gamma \ll 1$), which features a smooth temperature crossover from an incoherent gas, to a quasi-condensate, and, finally, at sufficiently low temperatures, to a ‘true’ condensate. This work complements earlier work in this area, which studied the interplay between density and phase fluctuations.

Results for the off-diagonal normalized first order correlation function were shown to be practically indistinguishable from those of a mean field theory which is valid in low dimensions and explicitly includes density fluctuations. This should be contrasted to theories which a priori ignore density fluctuations, with such theories shown to predict a larger amount of coherence than is physically present. Two different approximations for the evaluation of this correlation function were used, corresponding to different interference experiments that could be performed, and their profiles were shown to be very similar within the appropriate spatial range. We further investigated the temperature crossover in the shape of the correlation function, which evolves from gaussian to exponential with increasing temperature, and used this to obtain a monotonically varying coherence length.

Moreover, second and third order correlation functions at the same point were investigated as a function of temperature and interaction strength. The observed decrease in coherence when either of these parameters is increased was shown to be consistent with other results in the literature. Importantly, consideration of density-density correlations was shown to lead to an accurate determination of the quasi-condensate and thermal density profiles. This approach could be used in experiments, to provide a more accurate determination of quasi-condensate profiles and fractions, offering an alternative to the bimodal fitting schemes currently used.

In addition to providing valuable information for equilibrium profiles, to which the present analysis was restricted, the stochastic approach is well-suited for discussing growth of coherence in quasi-one-dimensional Bose gases, an issue that will be addressed in subsequent work.

Acknowledgments

It is a pleasure to acknowledge numerous discussions with Henk Stoof which have significantly contributed to the present work.

APPENDIX A: LOW-DIMENSIONAL MEAN FIELD THEORIES

This Appendix summarizes the modified finite temperature mean field theory of Andersen, Al Khawaja and

Stoof [22]. This theory extends alternative approaches suited to low-dimensional gases [21, 26] by providing an ab initio self-consistent treatment of density and phase fluctuations, which yields an equation of state free of both infrared and ultraviolet divergences. This theory is valid both for homogeneous and trapped systems in *all* dimensions, and has been shown to be consistent with well-known results in the appropriate limits [23]. Furthermore, such an approach enables a direct determination of quasi-condensate density profiles.

In the harmonic trap, one obtains an appropriate finite temperature nonlinear Schrödinger equation for the quasi-condensate, coupled to the Bogoliubov-de Gennes equations for the excitations. Solving these self-consistently within the Thomas-Fermi approximation yields a mean field approximation for the quasi-condensate spatial extent. This is referred to as the temperature-dependent Thomas-Fermi radius, and is denoted by $R_{\text{TF}}(T)$. This quantity depends on the quasi-condensate depletion $n'(z) = n_{\text{T}}(z)$, via $R_{\text{TF}}(T) = \sqrt{2\mu'/m\omega_z^2}$ where $\mu' = \mu - 2\kappa n'(0)$ is the ‘renormalized’ chemical potential. Here κ is the effective 1D coupling constant which is fixed by the atom mass, m , the 3D scattering length, $a_{3\text{D}}$, and the transverse confining frequency ω_{\perp} via $\kappa = a_{3\text{D}}/2\pi\ell_{\perp}^2$, where $\ell_{\perp} = \sqrt{\hbar/m\omega_{\perp}}$ is the harmonic oscillator length in the transverse direction [65]. Density profiles are obtained from the above equations in the local density approximation, with thermal profiles outside the quasi-condensate region obtained by solving the equation of state for the normal gas.

The first-order correlation function can be written as $g^{(1)}(0, z) = \exp\left(-\langle[\hat{\chi}(z) - \hat{\chi}(0)]^2\rangle/2\right)$, where $\hat{\chi}(z)$ is the operator for the phase, defined by expressing the Bose field operator $\hat{\Psi}(z)$ in the density-phase representation as $\hat{\Psi}(z) = \sqrt{n(z)}\exp\{i\hat{\chi}(z)\}$. In the theory of Andersen et al. [22], where density fluctuations are explicitly taken into consideration, the above exponent assumes,

in the purely one-dimensional geometry considered here, the following form

$$\langle[\hat{\chi}(z) - \hat{\chi}(0)]^2\rangle = \frac{4\pi\kappa l_z^4}{R_{\text{TF}}^3(T)} \sum_{j=0} 2N(\hbar\omega_j) \quad (\text{A1})$$

$$\left[A_j^2 (P_j(z/R_{\text{TF}}(T)) - P_j(0))^2 - B_j^2 \left(\frac{P_j(z/R_{\text{TF}}(T))}{1 - (z/R_{\text{TF}}(T))^2} - P_j(0) \right)^2 \right].$$

Here $P_j(z)$ are Legendre polynomials of order j , with $A_j = \sqrt{(j+1/2)\mu'/\hbar\omega_j}$, and $B_j = (\sqrt{(j+1/2)\hbar\omega_j/\mu'})/2$. The frequencies are given by $\omega_j = \sqrt{j(j+1)/2} \omega_z$, where l_z is the harmonic oscillator length corresponding to a longitudinal confining frequency ω_z . $N(\hbar\omega_j)$ is the usual Bose distribution function.

The appearance of the temperature-dependent quasi-condensate size $R_{\text{TF}}(T)$ in the prefactor ensures that density fluctuations are explicitly maintained in the above expression. The general expression quoted above can be readily reduced to the conventional theory which ignores quasi-condensate depletion [21, 26] by replacing $R_{\text{TF}}(T)$ by the corresponding zero temperature quasi-condensate size $R_{\text{TF}}(0)$ at the same *total* atom number, and ignoring the B_j contributions. Since $R_{\text{TF}}(T) \propto \sqrt{\mu'}$, the former step is equivalent to replacing the renormalized chemical potential at temperature T by the corresponding zero-temperature one for the same total atom number. Then, the ‘classical’ approximation $N(\hbar\omega_j) \approx k_B T/\hbar\omega_j$ leads to the definition of the characteristic temperature $T_{\phi} = (\hbar\omega_z)^2 N/k_B \mu$ [21].

For more details on the implementation of this theory to trapped gases, the reader is referred to [22, 23, 24, 25].

-
- [1] A. Görlitz, J.M. Vogels, A.E. Leanhardt, C. Raman, T.L. Gustavson, J.R. Abo-Shaeer, A.P. Chikkatur, S. Gupta, S. Inouye, T. Rosenband and W. Ketterle, Phys. Rev. Lett. **87**, 130402 (2001).
 - [2] F. Schreck, L. Khaykovich, K.L. Corwin, G. Ferrari, T. Bourdel, J. Cubizolles and C. Salomon, Phys. Rev. Lett. **87**, 080403 (2001).
 - [3] S. Dettmer, D. Hellweg, P. Ryytty, J.J. Arlt, W. Ertmer, K. Sengstock, D. S. Petrov, G. V. Shlyapnikov, H. Kreutzmann, L. Santos, and M. Lewenstein, Phys. Rev. Lett. **87**, 160406 (2001).
 - [4] I. Shvarchuck, Ch. Buggle, D.S. Petrov, K. Dieckmann, M. Zielonkowski, M. Kemmann, T.G. Tiecke, W. von Klitzing, G.V. Shlyapnikov, and J.T.M. Walraven, Phys. Rev. Lett. **89**, 270404 (2002).
 - [5] D. Hellweg, L. Cacciapiuoti, M. Kottke, T. Schulte, K. Sengstock, W. Ertmer, and J.J. Arlt, Phys. Rev. Lett. **91**, 010406 (2003).
 - [6] S. Richard, F. Gerbier, J.H. Thywissen, M. Hugbart, P. Bouyer, and A. Aspect, Phys. Rev. Lett. **91**, 010405 (2003).
 - [7] T.P. Meyrath, F. Schreck, J.L. Hanssen, C.-S. Chuu and M.G. Raizen, Phys. Rev. A **71**, 041604 (2005).
 - [8] B. Eiermann, P. Treutlein, Th. Anker, M. Albiez, M. Taglieber, K.-P. Marzlin, and M.K. Oberthaler Phys. Rev. Lett. **91**, 060402 (2003).
 - [9] H. Ott, J. Fortagh, G. Schlotterbeck, A. Grossmann, and C. Zimmermann, Phys. Rev. Lett. **87**, 230401 (2001).
 - [10] W. Hänsel, P. Hommelhoff, T. W. Hänsch, and J. Reichel, Nature **413**, 501 (2001).
 - [11] A. Leanhardt, A.P. Chikkatur, D. Kielpinski, Y. Shin, T.L. Gustavson, W. Ketterle, and D.E. Pritchard, Phys. Rev. Lett. **89**, 040401 (2002).
 - [12] S. Schneider, A. Kasper, Ch. vom Hagen, M. Bartenstein, B. Engeser, T. Schumm, I. Bar-Joseph, R. Folman, L. Feenstra and J. Schmiedmayer, Phys. Rev. A **67**, 023612 (2003).

- (2003).
- [13] M.P.A. Jones, C.J. Vale, D. Sahagun, B.V. Hall and E.A. Hinds, Phys. Rev. Lett. **91**, 080401 (2003).
 - [14] D. M. Harber, J. M. McGuirk, J. M. Obrecht, and E. A. Cornell, J. Low Temp. Phys. **133**, 229 (2003).
 - [15] Y.-J. Lin, I. Teper, C. Chin, and V. Vuletic Phys. Rev. Lett. **92**, 050404 (2004).
 - [16] J. Esteve, C. Aussibal, T. Schumm, C. Figl, D. Mailly, I. Bouchoule, C.I. Westbrook and A. Aspect, Phys. Rev. A **70**, 043629 (2004).
 - [17] C.J. Vale, B. Upcroft, M.J. Davis, N.R. Heckenberg and H. Rubinsztein-Dunlop, J. Phys. B **37**, 2959 (2004).
 - [18] New developements in atom chip technology can be found collected in a Special Issue - Atom Chips: manipulating atoms and molecules with micro-fabricated structures, C. Henkel, J. Schmiedmayer and C. Westbrook (Eds.) Eur. Phys. J. D **35** (2005).
 - [19] P. Krüger, L.M. Andersson, S. Wildermuth, S. Hofferberth, E. Haller, S. Aigner, S. Groth, I. Bar-Joseph and J. Schmiedmayer, cond-mat/0504686.
 - [20] V. N. Popov, Theor. Math. Phys. **11**, 565 (1972); *Functional Integrals in Quantum Field Theory and Statistical Physics*, (Reidel, Dordrecht, 1983), Chap. 6.
 - [21] D. S. Petrov, G.V. Shlyapnikov, and J.T.M. Walraven, Phys. Rev. Lett. **85**, 3745 (2000).
 - [22] J. O. Andersen, U. Al Khawaja, and H. T. C. Stoof, Phys. Rev. Lett. **88**, 070407 (2002).
 - [23] U. Al Khawaja, J.O. Andersen, N.P. Proukakis, and H.T.C. Stoof, Phys. Rev. A **66**, 013615 (2002); *ibid.* **66**, 059902(E) (2002).
 - [24] U. Al Khawaja, N.P. Proukakis, J.O. Andersen, M.W.J. Romans, and H.T.C. Stoof, Phys. Rev. A **68**, 043603 (2003).
 - [25] N.P. Proukakis, Phys. Rev. A **73**, 023605 (2006).
 - [26] D.L. Luxat and A. Griffin, Phys. Rev. A **67**, 043603 (2003).
 - [27] C. Mora and Y. Castin, Phys. Rev. A **67**, 053615 (2003).
 - [28] T.K. Ghosh, cond-mat/0402079.
 - [29] F. Gerbier, J.H. Thywissen, S. Richard, M. Hugbart, P. Bouyer and A. Aspect, Phys. Rev. A **67**, 051602 (2003).
 - [30] N.M. Bogoliubov, C. Malyshev, R.K. Bullough, and J. Timonen, Phys. Rev. A **69**, 023619 (2004).
 - [31] F. Gerbier, Europhys. Lett. **66**, 771 (2004).
 - [32] D. Kadio, M. Gajda and K. Rzazewski, Phys. Rev. A **72**, 013607 (2005).
 - [33] L. Cacciapuoti, D. Hellweg, M. Kottke, T. Schulte, W. Ertmer, J.J. Arlt, K. Sengstock, L. Santos and M. Lewenstein, Phys. Rev. A **68**, 053612 (2003).
 - [34] M. Hugbart, J. Retter, F. Gerbier, A. Varon, S. Richard, J. Thywissen, D. Clement, P. Bouyer, and A. Aspect, Eur. Phys. J. D **35**, 155 (2005).
 - [35] J. Esteve, J.-B. Trebbia, T. Schumm, A. Aspect, C. Westbrook, and I. Bouchoule, Phys. Rev. Lett. **96**, 130403 (2006).
 - [36] R.J. Glauber, Phys. Rev. **130**, 2529 (1963).
 - [37] R. Loudon, **The Quantum Theory of Light**, Second Edition (Clarendon Press, Oxford 1994).
 - [38] M.O. Scully and M.S. Zubairy, **Quantum Optics** (Cambridge University Press, 1997).
 - [39] C. Cohen-Tannoudji and C. Robilliard, C.R. Acad. Sci. Paris, t. 2, Serie IV, 445 (2001).
 - [40] M.D. Lee et al., cond-mat/0305416(2003).
 - [41] R. Walser, cond-mat/0411483 (2004).
 - [42] D.S. Petrov, G.V. Shlyapnikov and J.T.M. Walraven, Phys. Rev. Lett. **87**, 050404 (2001).
 - [43] H.T.C. Stoof, J. Low Temp. Phys. **114**, 11 (1999).
 - [44] H. T. C. Stoof and M.J. Bijlsma, J. Low Temp. Phys. **124**, 431 (2001).
 - [45] P.B. Blakie and M.J. Davis, Phys. Rev. A **72**, 063608 (2005).
 - [46] K.V. Kheruntsyan, D.M. Gangardt, P.D. Drummond and G.V. Shlyapnikov, Phys. Rev. A **71**, 053615 (2005).
 - [47] M.O. Mewes et al, Phys. Rev. Lett. **77**, 416 (1996).
 - [48] M. Holland et al., Phys. Rev. Lett. **78**, 3801 (1997).
 - [49] B.D. Busch, C. Liu, Z. Dutton, C.H. Behroozi and L.V. Hau, Europhys. Lett. **51**, 485 (2000).
 - [50] E.A. Burt et al., Phys. Rev. Lett. **79**, 337 (1997).
 - [51] Y. Kagan, B.V. Svistunov and G.V. Shlyapnikov, JETP Lett. **42**, 209 (1985).
 - [52] R. Hanbury Brown and R.Q. Twiss, Nature **177**, 27 (1956); *ibid.* **178**, 1046 (1956).
 - [53] S. Fölling, F. Gerbier, A. Widera, O. Mandel, T. Gericke and I. Bloch, Nature **434**, 481 (2005).
 - [54] M. Schellekens, R. Hoppeler, A. Perrin, J. Viana Gomes, D. Boiron, A. Aspect and C.I. Westbrook, Science **310**, 648 (2005).
 - [55] M. Greiner, C.A. Regal, J.T. Stewart and D.S. Jin, Phys. Rev. Lett. **94**, 110401 (2005).
 - [56] A. Öttl, S. Ritter, M. Köhl and T. Esslinger, Phys. Rev. Lett. **95**, 090404 (2005).
 - [57] K.V. Kheruntsyan, D.M. Gangardt, P.D. Drummond and G.V. Shlyapnikov, Phys. Rev. Lett. **91**, 040403 (2003).
 - [58] N.P. Proukakis, J. Schmiedmayer and H.T.C. Stoof, Phys. Rev. A **73**, 053603 (2006).
 - [59] N.P. Proukakis, Las. Phys. **13**, 527 (2003).
 - [60] C.W. Gardiner, J.R. Anglin and T.I.A. Fudge, J. Phys. B **35**, 1555 (2002).
 - [61] C.W. Gardiner and M.J. Davis, J. Phys. B **36**, 4732 (2003).
 - [62] M.J. Davis, S.A. Morgan and K. Burnett, Phys. Rev. Lett. **87**, 160402 (2001).
 - [63] A. Sinatra, C. Lobo and Y. Castin, Phys. Rev. Lett. **87**, 210404 (2001).
 - [64] M. Hugbart, J.A. Retter, A.F. Varon, P. Bouyer, A. Aspect and M.J. Davis, cond-mat/0602346 (2006).
 - [65] M. Olshanii, Phys. Rev. Lett. **81**, 938 (1998).
 - [66] S. Inouye, M.R. Andrews, J. Stenger, H.-J. Miesner, D.M. Stamper-Kurn and W. Ketterle, Nature **392**, 151 (1998).
 - [67] J.L. Roberts, N.R. Claussen, J.P. Burke, Jr., C.H. Greene, E.A. Cornell and C.E. Wieman, Phys. Rev. Lett. **81**, 5109 (1998).